

Spinon heat transport in the three-dimensional quantum magnet $\text{PbCuTe}_2\text{O}_6$

Xiaochen Hong^{1,2}, Matthias Gillig², Abanoub R. N. Hanna^{3,4}, Shravani Chillal⁴,
A. T. M. Nazmul Islam⁴, Bella Lake^{3,4}, Bernd Büchner^{2,5}, Christian Hess^{1,2,*}

¹*Fakultät für Mathematik und Naturwissenschaften,
Bergische Universität Wuppertal,
Gaußstraße 20, 42119 Wuppertal, Germany*

²*Leibniz-Institute for Solid State and Materials Research (IFW-Dresden),
Helmholtzstraße 20, 01069 Dresden, Germany*

³*Institut für Festkörperforschung,
Technische Universität Berlin,
Hardenbergstr. 36, 10623 Berlin, Germany*

⁴*Helmholtz-Zentrum Berlin für Materialien und Energie,
Hahn-Meitner Platz 1, 14109 Berlin, Germany*

⁵*Institute of Solid State and Materials Physics and Würzburg-Dresden Cluster of Excellence et.qmat,
Technische Universität Dresden, 01062 Dresden, Germany*

(Dated: November 22, 2023)

Quantum spin liquids (QSL) are novel phases of matter which remain quantum disordered even at the lowest temperature. They are characterized by emergent gauge fields and fractionalized quasiparticles. Here we show that the sub-Kelvin thermal transport of the three-dimensional $S = 1/2$ hyper-hyperkagome quantum magnet $\text{PbCuTe}_2\text{O}_6$ is governed by a sizeable charge-neutral fermionic contribution which is compatible with the itinerant fractionalized excitations of a spinon Fermi surface. We demonstrate that this hallmark feature of the QSL state is remarkably robust against sample crystallinity, large magnetic field, and field-induced magnetic order, ruling out the imitation of QSL features by extrinsic effects. Our findings thus reveal the characteristic low-energy features of $\text{PbCuTe}_2\text{O}_6$ which qualify this compound as a true QSL material.

Quantum spin liquid (QSL) states refer to highly entangled magnetic quantum ground states realized in frustrated magnets [1, 2]. Despite the quantum disorder of the ground states, the QSL possess well defined emergent fractionalized excitations such as spinons, Majorana fermions, visons, and many more [1–6], rendering them tantalizing since their initial proposal [7]. Recent years have witnessed the progress of materializing the QSL models [8], which has stimulated intense interest from both experimental and theoretical sides [3, 4]. By far most efforts in this field are devoted to two-dimensional systems because enhanced quantum fluctuations, an ingredient for realizing QSL states, are prominent in reduced dimensionality [2–4]. Nevertheless, there are also some three-dimensional (3D) QSL candidates. The most prominent model systems are examples of pyrochlore, hyperkagome, and double-layer kagome lattices [9–13].

Among the handful of candidate QSL materials, clear-cut evidence for the anticipated emergent fractionalized magnetic excitations, in particular the spinons, is rather scarce [3, 4]. Thermal conductivity, a probe only sensitive to itinerant entropy carriers, is the method of choice to prove the existence of spinons via their fermionic nature and their mobility [14, 15]. These important pieces of information are difficult to diagnose by thermodynamic or spectroscopic studies. To be specific, the spinon contri-

bution to the heat conductivity κ_{spinon} is expected to be linear in temperature (T) towards $T \rightarrow 0$ K [15], reminiscent of the electronic κ_e in metals. Except some one-dimensional spin-chain systems [16–18], compelling experimental evidence for this sought-after κ_{spinon} signalling a spinon Fermi surface is still pending. Earlier reports for κ_{spinon} in other QSL candidate materials have been shown to suffer from irreproducibility [19–23]. Some other QSL-like results can actually be explained by a peculiar phononic background resulting from spin scattering [24–27]. It is also argued that defects and impurities in a genuine QSL material can easily eliminate its fingerprints in thermal transport [23, 28, 29], preventing a reconciliation with other experimental techniques with which disorders do just the opposite, producing fraudulent QSL-like results in trivial systems [30–32]. It is therefore essential to exclude all these problems in order to reveal a true evidence for fermionic spinon heat transport, κ_{spinon} .

Cholalite $\text{PbCuTe}_2\text{O}_6$ crystallizes into a cubic P4_132 structure at ambient temperature [33, 34]. Its magnetic Cu^{2+} ions ($S = 1/2$) constitute a 3D network, similar to the Ir^{4+} ions in the hyperkagome material $\text{Na}_4\text{Ir}_3\text{O}_8$ [10]. However, density function theory calculations of $\text{PbCuTe}_2\text{O}_6$ suggest its nearest neighbor ($J_1 = 1.13$ meV, giving isolated triangles) and next nearest neighbor ($J_2 = 1.07$ meV, giving a hyperkagome lattice) interactions are almost of the same strength [35]. As a result, each Cu^{2+} ion is at the corner of three tri-

*c.hess@uni-wuppertal.de

angles rather than two triangles as for the hyperkagome case. The Cu^{2+} lattice of $\text{PbCuTe}_2\text{O}_6$ thus possesses 4-site and 6-site loops as its shortest spin rings [35], distinct from the 10-site loop of a standard hyperkagome lattice [36, 37], and was referred to as hyper-hyperkagome lattice [35]. An antiferromagnetic Curie-Weiss temperature $\Theta_{\text{CW}} \approx -22$ K was inferred from the magnetic susceptibility data of $\text{PbCuTe}_2\text{O}_6$ [34], but no magnetic order has been found down to 20 mK (frustration parameter $f = |\Theta_{\text{CW}}/T_N| > 1000$, where T_N is the Néel temperature) [34, 35, 38]. $\text{PbCuTe}_2\text{O}_6$ possesses a ferroelectric (FE) transition at around 1 K, accompanied by a structural transition to a lower symmetry phase [39, 40]. Notably, both the FE and structural distortions are absent in small-grained polycrystalline samples [39]. Regardless of this difference, characteristic multi-spinon continua of the magnetic excitations were identified by inelastic neutron scattering in both polycrystalline and single crystalline $\text{PbCuTe}_2\text{O}_6$ samples [35], down to 100 mK (below T_{FE}). This places $\text{PbCuTe}_2\text{O}_6$ on the shortlist of promising QSL materials with emergent spinon excitations.

In this Letter, we report clear evidences of spinon heat transport in this 3D QSL candidate material, $\text{PbCuTe}_2\text{O}_6$, at very low temperature, revealed by a sizeable T -linear contribution (κ_{spinon}) to the total thermal conductivity κ , which adds to the well-known T^3 contribution of phonons (κ_{ph}) [41]. Three different batches of $\text{PbCuTe}_2\text{O}_6$ samples prepared by different techniques, namely two differently fabricated single crystals and one polycrystalline sample were involved in this study [42]. κ of all samples has been studied at $T < 1$ K as well as at $6 \text{ K} \leq T \leq 160 \text{ K}$ [42]. In spite of a rich $H - T$ phase diagram of $\text{PbCuTe}_2\text{O}_6$, the signature of spinon heat transport is robust in all samples across the investigated parameter range.

As presented in Fig. 1(a), the low- T $\kappa(T)$ of the single crystalline Sample S1 at zero field shows distinct fingerprints of a spinon Fermi surface, *i.e.* a linear contribution to κ . This can easily be seen from the figure which shows the measured κ/T versus T^2 . In this representation, the linear contribution on top of a standard phononic background ($\kappa_{\text{ph}} \propto T^3$ [43]) is just the residual at 0 K [15]. Indeed, above a certain $T_{\text{drop}} \approx 340$ mK, the data can be well fitted according to $\kappa/T = a + b \times T^2$. Here $bT^2 \equiv \kappa_{\text{ph}}/T$ yields the expected phononic background with $b = 0.206 \text{ mW}/(\text{K}^4\text{cm})$ [44]. The residual $a = 0.075 \text{ mW}/(\text{K}^2\text{cm})$, as indicated by the red dot, represents a fermionic contribution to the heat conductivity. For insulating magnets such as $\text{PbCuTe}_2\text{O}_6$, such a fermionic contribution can only be explained by pertinent fractionalized magnetic excitations [14, 19]. The data thus provide clear-cut evidence for a spinon contribution, $\kappa_{\text{spinon}} \equiv aT$.

Our above conclusion of spinon heat transport and its quantitative determination is corroborated by our measurements of κ/T in magnetic fields. Fig. 1(b) shows

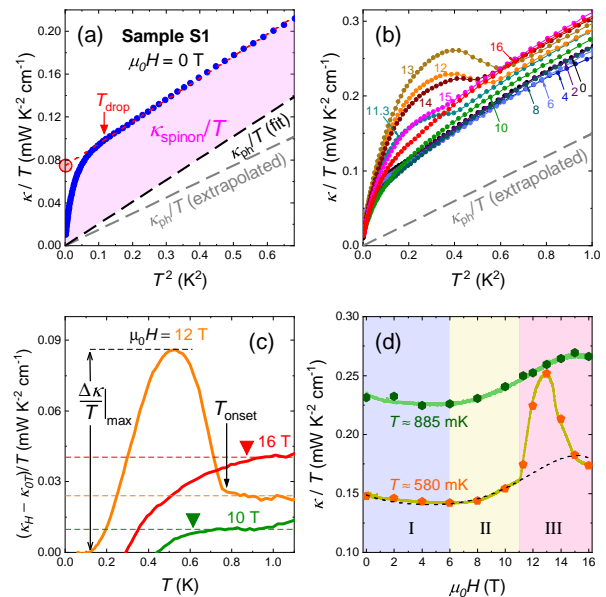


FIG. 1: (a) κ/T versus T^2 of Sample S1 in zero field, and extraction of κ_{ph} and κ_{spinon} , see text. The red dotted line represents a linear fit to κ/T above T_{drop} (red arrow), and its extrapolation to $T = 0$, yielding the linear residual $a \equiv \kappa_{\text{spinon}}/T$ (red dot). The dashed black line represents the thus extracted κ_{ph}/T . The spinon contribution κ_{spinon}/T on top of κ_{ph}/T is highlighted as the magenta region. The dashed gray line represents the extrapolated κ_{ph}/T from the $\kappa(T)$ data above 6 K [42, 44]. (b) $\kappa/T(T^2)$ in field together with the same extrapolated κ_{ph}/T curve as in panel (a). (c) Field effect on κ for three representative field values after subtracting the zero field value ($\kappa_H - \kappa_{0T}$)/ T . T_{drop} is highlighted by triangles, and the definition of the peak height ($\frac{\Delta\kappa}{T}|_{\text{max}}$) is exemplified. (d) Field dependence of κ/T isotherms measured at two selected temperatures (thick solid lines), plotted with the results (full symbols) extracted from the fixed-field $\kappa(T)/T$ data. Three different regions can be identified and are displayed by the different background colours. The black dashed line represents the higher temperature isotherm (green band) subtracted by a fixed value of $0.085 \text{ mW}/(\text{K}^2\text{cm})$, see text.

$\kappa/T(T)$ of Sample S1 in magnetic fields up to $\mu_0 H = 16$ T, with the field applied perpendicular to the heat current. The curves are only slightly affected by the field up to $\mu_0 H = 10$ T, and are shifted up with a nearly unaltered bT^2 term at higher fields. This renders our data fundamentally different from recently claimed evidences for a spinon residual κ_{spinon}/T term in several QSL candidate materials [24–26], where a large magnetic field leads to a strong enhancement (factor 2...10) of κ and bT^2 [27, 45, 46]. Contrastingly, the practically field independent bT^2 term in $\text{PbCuTe}_2\text{O}_6$ and the fact that the pure $\kappa_{\text{ph}}/T(T)$ curve is well below the total $\kappa/T(T)$ curves leave no room for a phononic-only explanation to the residual a as found in other frustrated magnets [27], confirming the κ_{spinon} transport channel.

We point out that while κ_{ph} remains weakly affected

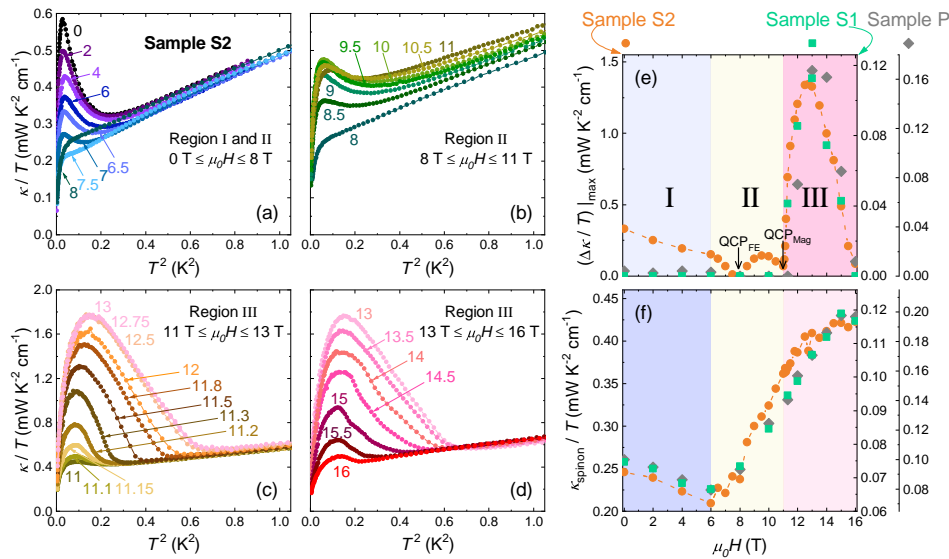


FIG. 2: The $\kappa/T(T^2)$ curves of Sample S2, separated into four panels (a-d) for clarity. The field dependence of the extracted amplitude of (e) the peaks and (f) the residual linear term κ_0/T are compared between all samples. The ferroelectric (QCP_{FE}) and magnetic (QCP_{Mag}) critical points [47] are marked by the black arrows. Note for the distinct ordinates with different scales. The determination of field regions is inherited from Fig. 1(d).

by the magnetic field, it still has a clear impact on the total κ . Firstly, as represented by the 12 T curve in Fig. 1(c) and also visible directly in Fig. 1(b), an additional $\kappa/T(T)$ peak on top of the phonon and spinon contributions emerges below T_{onset} in the field range of $11 T < \mu_0 H < 15 T$. Both the T_{onset} and the amplitude of the new peak are highly field sensitive. Eventually, at $\mu_0 H = 16 T$ the peak is absent again and the low field behavior of $\kappa/T(T)$ is recovered with a rather higher value of $T_{\text{drop}} \approx 870$ mK. Secondly, T_{drop} , which apparently represents an energy scale above which κ_{spinon} can be observed, increases with the field. As an example shown in Fig. 1(c), $T_{\text{drop}} \approx 610$ mK at $\mu_0 H = 10 T$. Finally, the residual $a \equiv \kappa_{\text{spinon}}/T$, increases considerably in this high field region above 10 T.

The general field evolution of κ/T is more clearly presented in Fig. 1(d) as $\kappa/T(H)$ isotherms. The high- T (885 mK, above T_{onset}) isotherm shows a minor decrease at small fields, followed by a slight continuous increase of κ/T above $\mu_0 H \approx 6 T$, until its saturation around $\mu_0 H = 15 T$. This increment is entirely due to κ_{spinon} , as was discussed above. On the other hand, the lower- T (580 mK, below T_{onset}) isotherm is more complicated, featuring a large hump centered around 13 T. Three field regions can thus be discerned based on the isotherms. The $\kappa/T(H)$ isotherms first decrease mildly in Region I, and then increase somewhat faster in Region II. Region III is defined by the occurrence of the peak. It is worthwhile to point out that the two isotherms match nicely in Region I & II through shifting by a constant value of 0.085 mW/(K²cm), i.e., the difference in the phononic contribution $b \times [(0.885 \text{ K})^2 - (0.58 \text{ K})^2]$. This

fact strongly suggests a new contributor to κ comes into play below T_{onset} in Region III, which will be discussed further below.

In order to evaluate whether any of the observed heat transport phenomenology described above is affected by the ferroelectric and accompanying structural transitions at $T_{\text{FE}} \approx 1$ K, we performed another heat transport measurement on a sample lacking the FE transition, namely the unannealed polycrystalline Sample P. With regard to the heat transport, it behaves basically the same as the single crystalline Sample S1 in the same T and H parameter range [42]. Thus, our above observations represent the intrinsic phenomenology of $\text{PbCuTe}_2\text{O}_6$, which is apparently independent of the ferroelectric or structural transitions. Note, that our $\kappa/T(T)$ curves show no anomaly at around 1 K [42], in contrast to the specific heat, which underpins this statement [39, 40, 47, 48]. This finding is important, because it demonstrates that the inferred κ_{spinon} is unaffected by the symmetry reduction induced by the ferroelectric order and the accompanying structural phase transition. Hence, our conclusion of compatibility with a QSL ground state remains robust even if the subtle non-cubic distortion present in the single crystalline Sample S1 below 1 K is taken into account [40].

After having established the intrinsic low-temperature heat transport behaviour of $\text{PbCuTe}_2\text{O}_6$, we turn now to the single crystalline Sample S2 which (unlike the phase-pure samples Sample S1 and Sample P [42]) is known to contain small amount of non-magnetic $\text{Pb}_2\text{Te}_3\text{O}_8$ inclusions in an otherwise phase pure $\text{PbCuTe}_2\text{O}_6$ matrix [35, 39]. The most obvious difference of the $\kappa(T)/T$

curves of Sample S2, shown in Fig. 2(a-d), compared to Samples S1 and P is an additional $\kappa/T(T)$ peak below $\mu_0 H = 11$ T (in Region I&II). It is highly sensitive to H , as embodied more clearly in Fig. 2(e), where the extracted peak height of Sample S2 reveals a sharp dip at $\mu_0 H \approx 8$ T, exactly the field at which the ferroelectric transition is driven to its critical point ($H_{QCP(FE)} = 7.9$ T)[47]. On the other hand, it is insensitive to the boundary between Region I and Region II. At higher field, the additional peak is preempted by the feature bounded to Region III. Although the $\kappa/T(T)$ peak of Sample S2 in Region III is much more pronounced as compared to Sample S1 and P, their extracted contributions ($\Delta\kappa/T|_{max}$) match extremely well after normalizing the peaks by their maximum value at 13 T (see Fig. 2(e)). The field dependent spinon contribution κ_{spinon}/T is also extracted from the data set above T_{onset} , and compared between all three samples, as presented in Fig. 2(f). Again they fit very well modulo a proper rescaling factor. In all samples, the κ_{spinon}/T values at 16 T increase by 70% or more with respect to their 0 T values. Further theoretical investigations are required to rationalize this field dependence. At present, one may speculate that it results from a field-induced variation of the spinon band width [49], or a field-induced shift of the spinon chemical potential [50].

It is very revealing to plot our main findings together with a recently established thermodynamic $T - H$ phase diagram of the ferroelectric (T_{FE}), magnetic (T_M), and structural (T_S) orders at low- T [47], see Fig. 3. Clearly, the onsets of the additional $\kappa/T(T)$ peak in Region III ($\mu_0 H > 11$ T) matches with the thermodynamic magnetic ordering temperatures T_M [47]. Hence, the excess heat conductivity which causes the peak can unambiguously be attributed to magnon transport. Note that magnons obey a bosonic behavior and emerge from long-range magnetic order in contrast to the spinons. At lower fields, the presence of the excess $\kappa/T(T)$ peak is obviously sample dependent since it can only be resolved for Sample S2. Here, the onset temperature (T_{onset}) and the peak height (see Fig. 2(e)) track at $H < H_{QCP(FE)}$ the ferroelectric order (T_{FE}) at somewhat lower T and recover at $H_{QCP(FE)} < H < 11$ T in the structurally distorted phase. It is therefore closely connected with the symmetry reduction due to the ferroelectric order and/or the structural distortion. Since phonons clearly are not sensitive to this symmetry reduction (see above), this low- T peak must be of magnetic origin. Despite the fact that magnetic order could not be detected below 11 T in previous works [34, 35, 38–40, 47], we therefore assign also this peak to magnon transport. It is known that $\text{PbCuTe}_2\text{O}_6$ is proximate to magnetic order [38, 40], and our data indicate that the disordered crystal matrix in Sample S2 due to the $\text{Pb}_2\text{Te}_3\text{O}_8$ inclusions drives this sample to magnetic order at low T . Overall, the most exotic finding of this work, the spinon contribution to thermal transport,

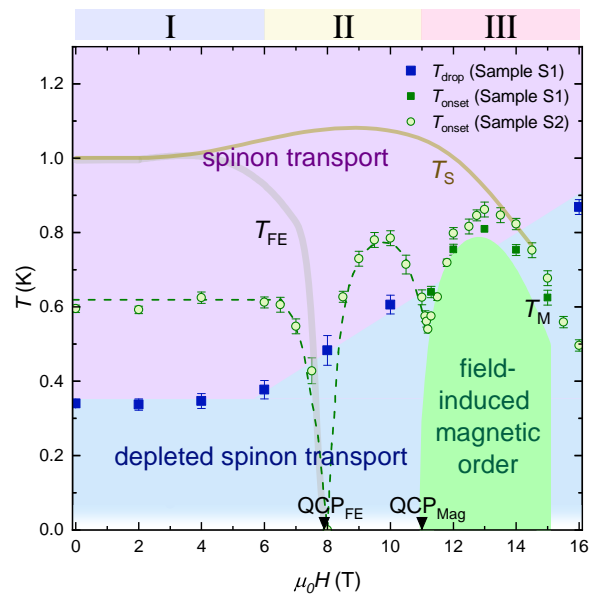


FIG. 3: Phase diagram of $\text{PbCuTe}_2\text{O}_6$, showing T_{onset} of samples S1 (green squares) and S2 (circles) as well as T_{drop} (sample S1) together with T_{FE} , T_S (dark yellow and grey lines), and T_M (top margin of light green area) as extracted from Ref. [47]. The ferroelectric QCP_{FE} at 7.9 T and magnetic QCP_{Mag} at 11 T are reproduced from Ref. [47]. The evidence for a quantum spin liquid state (i. e. finite residual linear term a) is not affected by the ferroelectric or structural transitions, thus is ubiquitous in the parameter space coloured in purple. The region below our experimental accessible range at $T \lesssim 50$ mK is left blank, except for the magnetically ordered phase.

prevails throughout the phase diagram until it is either freezing below T_{drop} , or is overshadowed by a magnetic order.

Finally, we address the freezing out of κ_{spinon}/T below T_{drop} . The depleted κ_{spinon} signal can either indicate a spinon excitation gap, or the loss of coupling between spinons and the phonon background [51], through which κ of an insulator is measured. Future work is required to clarify which of these two scenarios is valid (see [42]).

To summarize, the high-quality low- T thermal conductivity of a 3D QSL candidate $\text{PbCuTe}_2\text{O}_6$ strongly suggests the existence of itinerant spinons, and thus of a spinon Fermi surface. The spinon heat transport is shown to be intrinsic and robust against disorder and field-induced phases. Our work thus highlights $\text{PbCuTe}_2\text{O}_6$ as an unique model system for QSL research.

We acknowledge fruitful discussions with Wolfram Brenig, Elena Hassinger, and Matthias Vojta. We thank Michael Lang, Bernd Wolf, Paul Eibisch and Christian Thurn for ample discussions about our parallel going experiments and for sharing their thermodynamic results with us before publication. We further thank Tino Schreiner and Danny Baumann for technical assistance. This project has been supported by the Deutsche

Forschungsgemeinschaft through the Sonderforschungsbereich SFB 1143. Furthermore, this project has received funding from the European Research Council (ERC) under the European Unions' Horizon 2020 research and innovation programme (grant agreement No 647276 – MARS – ERC-2014-CoG).

-
- [1] L. Balents, Spin liquids in frustrated magnets. *Nature* **464**, 199–208 (2010). <https://doi.org/10.1038/nature08917>
- [2] L. Savary and L. Balents, Quantum spin liquids: a review. *Rep. Prog. Phys.* **80**, 106502 (2017). DOI 10.1088/0034-4885/80/1/016502
- [3] Y. Zhou, K. Kanoda, and T.K. Ng, Quantum spin liquid states. *Rev. Mod. Phys.* **89**, 025003 (2017). <https://doi.org/10.1103/RevModPhys.89.025003>
- [4] C. Broholm, R. J. Cava, S. A. Kivelson, D. G. Nocera, M. R. Norman, and T. Senthil, Quantum spin liquids. *Science* **367**, eaay0668 (2020). DOI: 10.1126/science.aay0668
- [5] X.-G. Wen, Quantum orders and symmetric spin liquids. *Phys. Rev. B* **65**, 165113 (2002). <https://doi.org/10.1103/PhysRevB.65.165113>
- [6] X.-G. Wen, Choreographed entanglement dances: Topological states of quantum matter. *Science* **363**, eaal3099 (2019). DOI: 10.1126/science.aal3099
- [7] P. W. Anderson, *Mater. Res. Bull.* **8**, 153–160 (1973). Resonating valence bonds: A new kind of insulator? [https://doi.org/10.1016/0025-5408\(73\)90167-0](https://doi.org/10.1016/0025-5408(73)90167-0)
- [8] P. A. Lee, An end to the drought of quantum spin liquids. *Science* **321**, 1306–1307 (2008). DOI: 10.1126/science.1163196
- [9] M. J. P. Gingras and P. A. McClarty, Quantum spin ice: a search for gapless quantum spin liquids in pyrochlore magnets. *Rep. Prog. Phys.* **77**, 056501 (2014). DOI 10.1088/0034-4885/77/5/056501
- [10] Y. Okamoto, M. Nohara, H. Aruga-Katori, and H. Takagi, Spin-liquid state in the $S = 1/2$ hyperkagome antiferromagnet $\text{Na}_4\text{Ir}_3\text{O}_8$. *Phys. Rev. Lett.* **99**, 137207 (2007). <https://doi.org/10.1103/PhysRevLett.99.137207>
- [11] C. Balz, B. Lake, J. Reuther, H. Luetkens, R. Schoneemann, T. Herrmannsdorfer, Y. Singh, A. T. M. N. Islam, E. M. Wheeler, J. A. Rodriguez-Rivera, T. Guidi, G. G. Simeoni, C. Baines, and H. Ryll, Physical realization of a quantum spin liquid based on a complex frustration mechanism. *Nat. Phys.* **12**, 942–949 (2016). <https://doi.org/10.1038/nphys3826>
- [12] K. W. Plumb, H. J. Changlani, A. Scheie, S. Zhang, J. W. Krizan, J. A. Rodriguez-Rivera, Y. Qiu, B. Winn, R. J. Cava, and C. L. Broholm, Continuum of quantum fluctuations in a three-dimensional $S = 1$ Heisenberg magnet. *Nat. Phys.* **15**, 54–59 (2019). <https://doi.org/10.1038/s41567-018-0317-3>
- [13] B. Gao, T. Chen, D. W. Tam, C.-L. Huang, K. Sasmal, D. T. Adroja, F. Ye, H. Cao, G. Sala, M. B. Stone, C. Baines, J. A. T. Verezhak, H. Hu, J.-H. Chung, X. Xu, S.-W. Cheong, M. Nallaiyan, S. Spagna, M. B. Maple, A. H. Nevidomskyy, E. Morosan, G. Chen, and P. C. Dai, Experimental signatures of a three-dimensional quantum spin liquid in effective spin-1/2 $\text{Ce}_2\text{Zr}_2\text{O}_7$ pyrochlore. *Nat. Phys.* **15**, 1052–1057 (2019). <https://doi.org/10.1038/s41567-019-0577-6>
- [14] S.-S. Lee, P. A. Lee, and T. Senthil, Amperian Pairing Instability in the U(1) Spin Liquid State with Fermi Surface and Application to κ -(BEDT-TTF) $_2\text{Cu}_2(\text{CN})_3$. *Phys. Rev. Lett.* **98**, 067006 (2007). <https://doi.org/10.1103/PhysRevLett.98.067006>
- [15] M. Yamashita, T. Shibauchi, and Y. Matsuda, Thermal-transport studies of two-dimensional quantum spin liquids. *Chem. Phys. Chem.* **13**, 74 (2012). <https://doi.org/10.1002/cphc.201100556>
- [16] C. Hess, H. ElHaes, A. Waske, B. Büchner, C. Sekar, G. Krabbes, F. Heidrich-Meisner, and W. Brenig, Linear Temperature Dependence of the Magnetic Heat Conductivity in CaCu_2O_3 . *Phys. Rev. Lett.* **98**, 027201 (2007). <https://doi.org/10.1103/PhysRevLett.98.027201>
- [17] B. Y. Pan, Y. Xu, J. M. Ni, S. Y. Zhou, X. C. Hong, X. Qiu, and S. Y. Li, Unambiguous Experimental Verification of Linear-in-Temperature Spinon Thermal Conductivity in an Antiferromagnetic Heisenberg Chain. *Phys. Rev. Lett.* **129**, 167201 (2022). <https://doi.org/10.1103/PhysRevLett.129.167201>
- [18] N. Hlubek, P. Ribeiro, R. Saint-Martin, A. Revcolevschi, G. Roth, G. Behr, B. Büchner, and C. Hess, Ballistic heat transport of quantum spin excitations as seen in SrCuO_2 . *Phys. Rev. B* **81**, 020405(R) (2010). <https://doi.org/10.1103/PhysRevB.81.020405>
- [19] M. Yamashita, N. Nakata, Y. Senshu, M. Nagata, H. M. Yamamoto, R. Kato, T. Shibauchi, and Y. Matsuda, Highly Mobile Gapless Excitations in a Two-Dimensional Candidate Quantum Spin Liquid. *Science* **328**, 1246–1248 (2010). DOI: 10.1126/science.1188200
- [20] J. M. Ni, B. L. Pan, B. Q. Song, Y. Y. Huang, J. Y. Zeng, Y. J. Yu, E. J. Cheng, L. S. Wang, D. Z. Dai, R. Kato, and S. Y. Li, Thermal conductivity of the quantum spin liquid candidate $\text{EtMe}_3\text{Sb}[\text{Pd}(\text{dmit})_2]_2$: No evidence of mobile gapless excitations. *Phys. Rev. Lett.* **123**, 247204 (2019). <https://doi.org/10.1103/PhysRevLett.123.247204>
- [21] P. Bourgeois-Hope, F. Laliberte, E. Lefrancois, G. Grissonnanche, S. Rene de Cotret, R. Gordon, S. Kitou, H. Sawa, H. Cui, R. Kato, L. Taillefer, and N. Doiron-Leyraud, Absence of magnetic thermal conductivity in the quantum spin liquid candidate $\text{EtMe}_3\text{Sb}[\text{Pd}(\text{dmit})_2]_2$. *Phys. Rev. X* **9**, 041051 (2019). <https://doi.org/10.1103/PhysRevX.9.041051>
- [22] Y. J. Yu, Y. Xu, L. P. He, M. Kratochvilova, Y. Y. Huang, J. M. Ni, L. Wang, S.-W. Cheong, J.-G. Park, and S. Y. Li, Heat transport study of the spin liquid candidate $1T\text{-TaS}_2$. *Phys. Rev. B* **96**, 081111(R) (2017). <https://doi.org/10.1103/PhysRevB.96.081111>
- [23] H. Murayama, Y. Sato, T. Taniguchi, R. Kurihara, X. Z. Xing, W. Huang, S. Kasahara, Y. Kasahara, I. Kimchi, M. Yoshida, Y. Iwasa, Y. Mizukami, T. Shibauchi, M. Konczykowski, and Y. Matsuda, Effect of quenched disorder on the quantum spin liquid state of the triangular-lattice antiferromagnet $1T\text{-TaS}_2$. *Phys. Rev. Research* **2**, 013099 (2020). <https://doi.org/10.1103/PhysRevResearch.2.013099>
- [24] N. Li, Q. Huang, X. Y. Yue, W. J. Chu, Q. Chen, E. S. Choi, X. Zhao, H. D. Zhou, and X. F. Sun, Possible itinerant excitations and quantum spin state transitions in the effective spin-1/2 triangular-lattice antiferromagnet $\text{Na}_2\text{BaCo}(\text{PO}_4)_2$. *Nat. Commun.* **11**, 4216 (2020).

- <https://doi.org/10.1038/s41467-020-18041-3>
- [25] X. Rao, G. Hussain, Q. Huang, W. J. Chu, N. Li, X. Zhao, Z. Dun, E. S. Choi, T. Asaba, L. Chen, L. Li, X. Y. Yue, N. N. Wang, J.-G. Cheng, Y. H. Gao, Y. Shen, J. Zhao, G. Chen, H. D. Zhou, and X. F. Sun, Survival of itinerant excitations and quantum spin state transitions in YbMgGaO_4 with chemical disorder. *Nat. Commun.* **12**, 4949 (2021). <https://doi.org/10.1038/s41467-021-25247-6>
- [26] S. Guang, N. Li, R. L. Luo, Q. Huang, Y. Wang, X. Yue, K. Xia, Q. Li, X. Zhao, G. Chen, H. Zhou, and X. Sun, Thermal transport of fractionalized antiferromagnetic and field-induced states in the Kitaev material $\text{Na}_2\text{Co}_2\text{TeO}_6$. *Phys. Rev. B* **107**, 184423 (2023). <https://doi.org/10.1103/PhysRevB.107.184423>
- [27] X. C. Hong, M. Gillig, W. L. Yao, L. Janssen, V. Kocsis, S. Gass, Y. Li, A. U. B. Wolter, B. Buchner, and C. Hess, Phonon thermal transport shaped by strong spin-phonon scattering in a Kitaev material $\text{Na}_2\text{Co}_2\text{TeO}_6$. *On-line preprint arXiv:2306.16963*
- [28] M. Yamashita, Y. Sato, T. Tominaga, Y. Kasahara, S. Kasahara, H. Cui, R. Kato, T. Shibauchi, and Y. Matsuda, Presence and absence of itinerant gapless excitations in the quantum spin liquid candidate $\text{EtMe}_3\text{Sb}[\text{Pd}(\text{dmit})_2]_2$. *Phys. Rev. B* **101**, 140407(R) (2020). <https://doi.org/10.1103/PhysRevB.101.140407>
- [29] Y. Y. Huang, Y. Xu, L. Wang, C. C. Zhao, C. P. Tu, J. M. Ni, L. S. Wang, B. L. Pan, Y. Fu, Z. Hao, C. Liu, J.-W. Mei, and S. Y. Li Heat Transport in Herbertsmithite: Can a Quantum Spin Liquid Survive Disorder? *Phys. Rev. Lett.* **127**, 267202 (2021). <https://doi.org/10.1103/PhysRevLett.127.267202>
- [30] Z. Zhu, P. A. Maksimov, S. R. White, and A. L. Chernyshev, Disorder-induced mimicry of a spin liquid in YbMgGaO_4 . *Phys. Rev. Lett.* **119**, 157201 (2017). <https://doi.org/10.1103/PhysRevLett.119.157201>
- [31] J. R. Chamorro, T. M. McQueen, and T. T. Tran, Chemistry of Quantum Spin Liquids. *Chem. Rev.* **121**, 2898–2934 (2021). <https://doi.org/10.1021/acs.chemrev.0c00641>
- [32] Z. Ma, Z.-Y. Dong, S. Wu, Y. Zhu, S. Bao, Z. Cai, W. Wang, Y. Shangguan, J. Wang, K. Ran, D. Yu, G. Deng, R. A. Mole, H.-F. Li, S.-L. Yu, J.-X. Li, and J. S. Wen, Disorder-induced spin-liquid-like behavior in kagome-lattice compounds. *Phys. Rev. B* **102**, 224415 (2020). <https://doi.org/10.1103/PhysRevB.102.224415>
- [33] D. S. Inosov, Quantum magnetism in minerals. *Adv. Phys.* **67**, 149–252 (2018). <https://doi.org/10.1080/00018732.2018.1571986>
- [34] B. Koteswararao, R. Kumar, P. Khuntia, S. Bhowal, S. K. Panda, M. R. Rahman, A. V. Mahajan, I. Dasgupta, M. Baenitz, K. H. Kim, and F. C. Chou Magnetic properties and heat capacity of the three-dimensional frustrated $S = 1/2$ antiferromagnet $\text{PbCuTe}_2\text{O}_6$. *Phys. Rev. B* **90**, 035141 (2014). <https://doi.org/10.1103/PhysRevB.90.035141>
- [35] S. Chillal, Y. Iqbal, H. O. Jeschke, J. A. Rodriguez-Rivera, R. Bewley, P. Manuel, D. Khalyavin, P. Steffens, R. Thomale, A. T. M. N. Islam, J. Reuther, and B. Lake, Evidence for a three-dimensional quantum spin liquid in $\text{PbCuTe}_2\text{O}_6$. *Nat. Commun.* **11**, 2348 (2020). <https://doi.org/10.1038/s41467-020-15594-1>
- [36] Y. Zhou, P. A. Lee, T.-K. Ng, and F.-C. Zhang, $\text{Na}_4\text{Ir}_3\text{O}_8$ as a 3D Spin Liquid with Fermionic Spinons. *Phys. Rev. Lett.* **101**, 197201 (2008). <https://doi.org/10.1103/PhysRevLett.101.197201>
- [37] E. J. Bergholtz, A. M. Lauchli, and R. Moessner, Symmetry breaking on the three-dimensional hyperkagome lattice of $\text{Na}_4\text{Ir}_3\text{O}_8$. *Phys. Rev. Lett.* **105**, 237202 (2010). <https://doi.org/10.1103/PhysRevLett.105.237202>
- [38] P. Khuntia, F. Bert, P. Mendels, B. Koteswararao, A. V. Mahajan, M. Baenitz, F. C. Chou, C. Baines, A. Amato, and Y. Furukawa, Spin liquid state in the 3D frustrated antiferromagnet $\text{PbCuTe}_2\text{O}_6$: NMR and Muon spin relaxation studies. *Phys. Rev. Lett.* **116**, 107203 (2016). <https://doi.org/10.1103/PhysRevLett.116.107203>
- [39] A. R. N. Hanna, A. T. M. N. Islam, R. Feyerherm, K. Siemensmeyer, K. Karmakar, S. Chillal, and B. Lake, Crystal growth, characterization, and phase transition of $\text{PbCuTe}_2\text{O}_6$. *Phys. Rev. Materials* **5**, 113401 (2021). <https://doi.org/10.1103/PhysRevMaterials.5.113401>
- [40] C. Thurn, P. Eibisch, A. Ata, M. Winkler, P. Lunkenheimer, I. Kezsmarki, U. Tutsch, Y. Saito, S. Hartmann, J. Zimmermann, A. R. N. Hanna, A. T. M. N. Islam, S. Chillal, B. Lake, B. Wolf, and M. Lang, Spin liquid and ferroelectricity close to a quantum critical point in $\text{PbCuTe}_2\text{O}_6$. *npj Quantum Mater.* **6**, 95 (2021). <https://doi.org/10.1038/s41535-021-00395-6>
- [41] P. D. Thacher, Effect of Boundaries and Isotopes on the Thermal Conductivity of LiF . *Phys. Rev.* **156**, 975 (1967). <https://doi.org/10.1103/PhysRev.156.975>
- [42] see Supplementary Material.
- [43] R. Berman, Thermal Conduction in Solids, The Clarendon Press, Oxford, (1976).
- [44] Attributing bT^3 to κ_{ph} is endorsed by the very good agreement of the fitted κ_{ph} and the extrapolated κ_{ph} (Fig. 1) from the high temperature κ data as an independent evaluation, which depends on the dominance of canonical κ_{ph} in $\text{PbCuTe}_2\text{O}_6$ at high enough temperatures [42].
- [45] M. Gillig, X. C. Hong, P. Sakrikar, G. Bastien, A. U. B. Wolter, L. Heinze, S. Nishimoto, B. Buchner, and C. Hess, Thermal transport of the frustrated spin-chain mineral linarite: Magnetic heat transport and strong spin-phonon scattering. *Phys. Rev. B* **104**, 235129 (2021). <https://doi.org/10.1103/PhysRevB.104.235129>
- [46] X. C. Hong, M. Behnami, L. Yuan, B. Li, W. Brenig, B. Buchner, Y. S. Li, and C. Hess, Heat transport of the kagome Heisenberg quantum spin liquid candidate $\text{YCu}_3(\text{OH})_{6.5}\text{Br}_{2.5}$: Localized magnetic excitations and a putative spin gap. *Phys. Rev. B* **106**, L220406 (2022). <https://doi.org/10.1103/PhysRevB.106.L220406>
- [47] P. Eibisch, C. Thurn, A. Ata, Y. Saito, S. Hartmann, U. Tutsch, B. Wolf, A. T. M. N. Islam, S. Chillal, A. R. N. Hanna, B. Lake, and M. Lang, Field-induced effects in the spin liquid candidate $\text{PbCuTe}_2\text{O}_6$. *Phys. Rev. B* **107**, 235133 (2023). <https://doi.org/10.1103/PhysRevB.107.235133>
- [48] We point out that a linear contribution is not observed in the heat capacity measurement in the sub-Kelvin regime [38–40], presumably because of the dominance of the entropy associated with the ferroelectric transition.
- [49] F. Forte, J. van den Brink, and M. Cuoco, Evolution of spinon Fermi surface and magnetic response of hyperkagome spin liquids. *Phys. Rev. B* **88**, 144422 (2013). <https://doi.org/10.1103/PhysRevB.88.144422>
- [50] Y. Shen, Y.-D. Li, H. C. Walker, P. Steffens, M. Boehm, X. Zhang, S. Shen, H. Wo, G. Chen, and J. Zhao, Frac-

tionalized excitations in the partially magnetized spin liquid candidate YbMgGaO_4 . *Nat. Commun.* **9**, 4138 (2018). <https://doi.org/10.1038/s41467-018-06588-1>

[51] M. F. Smith, J. Paglione, M. B. Walker, and L. Taillefer, Origin of anomalous low-

temperature downturns in the thermal conductivity of cuprates, *Phys. Rev. B* **71**, 014506 (2005). <https://doi.org/10.1103/PhysRevB.71.014506>

Supplementary Materials for:

Spinon heat transport in the three-dimensional quantum magnet $\text{PbCuTe}_2\text{O}_6$

I. Sample preparation

Polycrystalline powder of $\text{PbCuTe}_2\text{O}_6$ was synthesized by a solid-state reaction of high-purity powder of PbO , CuO , and TeO_2 . Sample P was produced from the as-grown stoichiometric polycrystalline powder, pressed and sintered in flowing argon for 12 h at 540 °C after the initial reaction. Sample P was not treated by a 5-days long annealing process which increases the grain size, thus it belongs to the small-grain polycrystal where no evident ferroelectric transition can be recognized [1]. It was cut into a rectangular bar of $3.13 \times 1.22 \times 0.2 \text{ mm}^3$. Sample S1, with a dimension of $1.87 \times 0.88 \times 0.72 \text{ mm}^3$, was cut from a single crystal synthesized by the top-seeded solution growth (TSSG) method. The crystal was grown using a Czochralski furnace under flowing Argon atmosphere. No inclusion of any impurity phase was detected in these TSSG-grown single crystals [2]. Sample S2, with a dimension of $3.06 \times 1.04 \times 0.75 \text{ mm}^3$, was cut from a single crystal synthesized by the traveling solvent floating zone (TSFZ) technique. The growths were performed under flowing Argon atmospheres. It is noticed that the TSFZ-grown crystals always contain 6% \sim 8% of non-magnetic impurity inclusions ($\text{Pb}_2\text{Te}_3\text{O}_8$) [1, 2]. The samples we studied are either the same (Sample S1) [3], or from the same batches (Sample S2 and Sample P) [1], of the samples used in other investigations. An exhaustive description of the growing conditions and characterizations can be found in the references [1, 2].

II. Details of the heat transport measurements

The thermal conductivities below liquid helium temperature were measured in a dilution refrigerator, using a standard four-wire steady-state method with two RuO_2 chip thermometers, calibrated *in situ* against a reference RuO_2 thermometer. The temperature gradient

was always applied along the longest direction of the sample. One end of the sample was glued directly to the heat sink. The temperature difference between two sensors was regulated to about 5% of the average sample temperature by a heater (10 k Ω) attached to the other end of the sample (see Fig. S1).

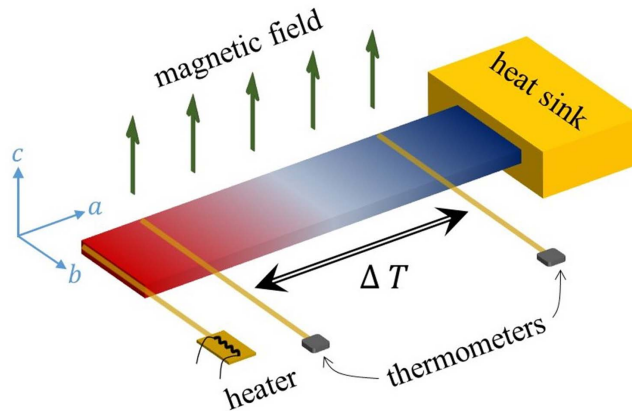


Fig. S1: A schematic sketch of the experimental setup. The magnetic field H was applied perpendicular to the heat current.

Samples were measured in a home-built probe for higher temperature thermal conductivity data. The temperature gradient was measured by a differential AuFe/chromel-P thermocouple which had been calibrated carefully in a magnetic field.

Being an isotropic three-dimensional Heisenberg magnet, $\text{PbCuTe}_2\text{O}_6$ should not be sensitive to field direction. For consistency, magnetic field was always applied perpendicular to the heat current.

The $\kappa(H)$ isotherms have been collected in a continuous manner. For each $\kappa(H)$ isotherm, the heat sink temperature was kept at a set point, and the heater was set to a constant value that is around half of its 0 T power of the $\kappa(T)$ measurement in order to minimise the impact of κ change on the actual sample temperature. The magnetic field was swept at a speed no more than 50 mT per minute to avoid any heating effect, in order to keep the system in a (quasi-)thermal equilibrium state. The data analysis procedure for the $\kappa(H)$ measurements is elaborated below.

III. Data analysis of the field ramp measurements

As for the field ramp measurements, the heat sink is set at a fixed temperature. The heating power is also fixed at a certain value. So, the temperature difference between the sensors is inversely proportional to the thermal conductivity. Of course, the (average) sample temperature also changes according to the field because of the conductivity variance. In order to reduce this effect, a relatively low heating power was applied to the sample. The field effect on the sample temperatures was below 2% for all the field ramp results we present in this work.

Ruthenium oxide (RuO_2) is generally believed as the prime choice for thermometry at low temperature, due to its high sensitivity and low magnetic field effect [4]. However, the magnetoresistance of RuO_2 at dilution fridge temperatures is not negligible (see Fig. S2(b)). In the field ramp measurements, the key challenge is to properly calibrate the temperature sensors in variant fields. Below we show our approach to achieve this goal.

As a semiconductor, the $R(T)$ curves of RuO_2 at fixed fields roughly follows the trend of

$$R(T, H) \propto \exp\left(\frac{-\Delta}{k_B T}\right) \quad (1)$$

It is also known that the magnetoresistance of RuO_2 at fixed temperature is roughly linear [4]

$$R(T, H) \approx R(T, H = 0) \times (1 + \alpha H) \quad (2)$$

By combining these two relationships together, one can expect the corresponding temperature of a certain resistance value at different magnetic fields follows

$$T(R, H) = T(R, H = 0 \text{ T}) + \beta \times \ln(H - \gamma) \quad (3)$$

In Fig. S2 we show one practical example step by step. The raw resistance values during one field ramp measurement is present in Fig. S2(a). At $H = 5 \text{ T}$, the resistance value reads $R = 3258.47\Omega$. Taking advantage of the self-calibration matrix of sensors we got during the fixed field measurements, this resistance value is converted to a list of temperatures at different fields, as shown in Fig. S2(b). These temperatures are plotted as green squares in Fig. S2(c). They fit well into Eq. S3, as the dashed blue curve indicates. According to that, $(R = 3258.47\Omega, H = 5 \text{ T})$ means this temperature sensor is at 628.6 mK.

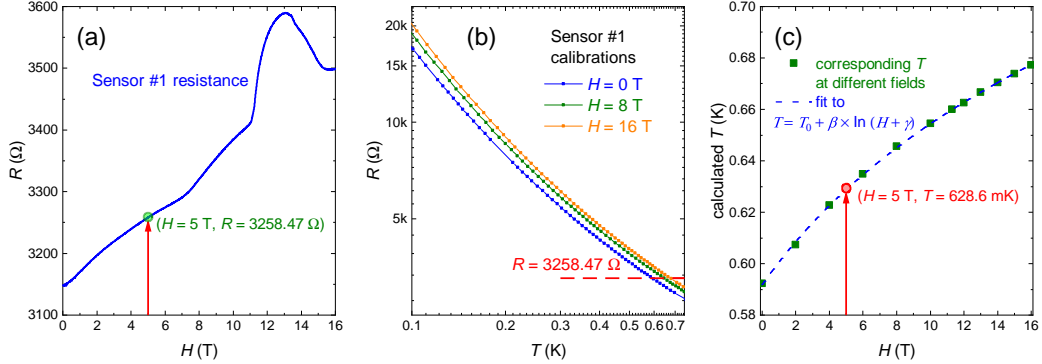


Fig. S2: Illustration of temperature sensor calibration in field. (a) Raw resistance data of one sensor in a field ramp measurement. The sensor reads 3258.47 Ω at $H = 5$ T. (b) Self-calibration curves of this sensor at different fields. Only three representative curves are shown for clarity. A clear magnetoresistance effect is observable. The corresponding T of $R = 3258.47$ Ω at a fixed field is the crossing point of the curve with the dashed red line. (c) The corresponding T of $R = 3258.47$ Ω is different at different fields. The dashed blue line is a fit to them according to Eq. S3. T_0 is set to $T(R = 3258.47 \text{ Ω}, H = 0 \text{ T})$. β , and γ are free fitting parameters.

Such procedure turns every (R, H) cluster of both sensors into T . Based on them, the thermal conductivity and sample temperature can be calculated. The resultant κ/T of the field ramp measurements match very well with the data extracted from the fixed field results, as evident in Fig. 1(d) of the main text. This fact rationalizes our data analysis procedure described above, and demonstrates the accuracy and reproducibility of our results.

IV. Modeling the phonon thermal transport

The thermal conductivity curves of both single crystals at $T > 6$ K show only one peak and no distinguishable field dependence (see Fig. S3). The absence of any field dependence proves the phonon-spin scattering is not important in $\text{PbCuTe}_2\text{O}_6$, in contrast to some other spin liquid candidate materials like $\alpha\text{-RuCl}_3$ [5]. $\text{PbCuTe}_2\text{O}_6$ is an electrical insulator, hence the measured field-independent κ at such temperature range is primarily phononic. The Callaway model is an established method to describe the phonon thermal conductivity [6, 7]. By applying a Debye ansatz for the phonon heat capacity, the expression for thermal

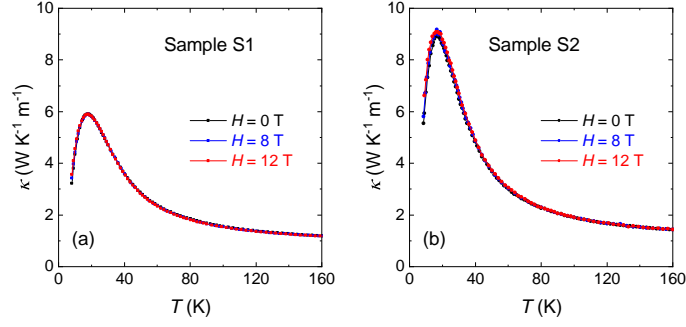


Fig. S3: Thermal conductivity of the two single crystals up to room temperature. κ versus T at zero and finite fields. (a) Sample S1 and (b) Sample S2.

conductivity is

$$\kappa(T) = \frac{k_B}{2\pi^2 v_s} \left(\frac{k_B T}{\hbar} \right)^3 \int_0^{\Theta_D/T} \frac{x^4 e^x}{(e^x - 1)^2} \tau_c(x) dx, \quad (4)$$

with frequency-dependent dimensionless energy ratio $x = \hbar\omega/k_B T$, the scattering time τ_c , the sound velocity v_s , and the Debye temperature Θ_D ($\Theta_D = 92$ K for $\text{PbCuTe}_2\text{O}_6$ [8]). The total scattering rate is contributed by different scattering mechanisms added up according to the Matthiessen's rule: $\tau_C^{-1} = \tau_U^{-1} + \tau_D^{-1} + \tau_B^{-1}$. The contributing phonon-boundary scattering $\tau_B^{-1} = v_s/L$, the phonon-defect scattering $\tau_D^{-1} = C\omega^4$ and the phonon-phonon scattering

$$\tau_U^{-1} = BT\omega^3 \exp\left(-\frac{\Theta_D}{\alpha T}\right), \quad (5)$$

are described by empirical expressions.

We use this model to phenomenologically fit our data in the temperature range of 6 K < T < 100 K. The obtained parameters are shown in Table S1 and the fitting results are depicted in Fig. S4(a-c).

Sample	B [10^{-30} K^{-1}s^2]	C [10^{-42} s^3]	L [10^{-6} m]	α
S1	3.56	2.75	5.49	2.82
S2	3.34	2.12	9.56	2.42
P	3.46	3.25	5.13	2.72

Table S1: Obtained fitting parameters of the Callaway model for the three different samples.

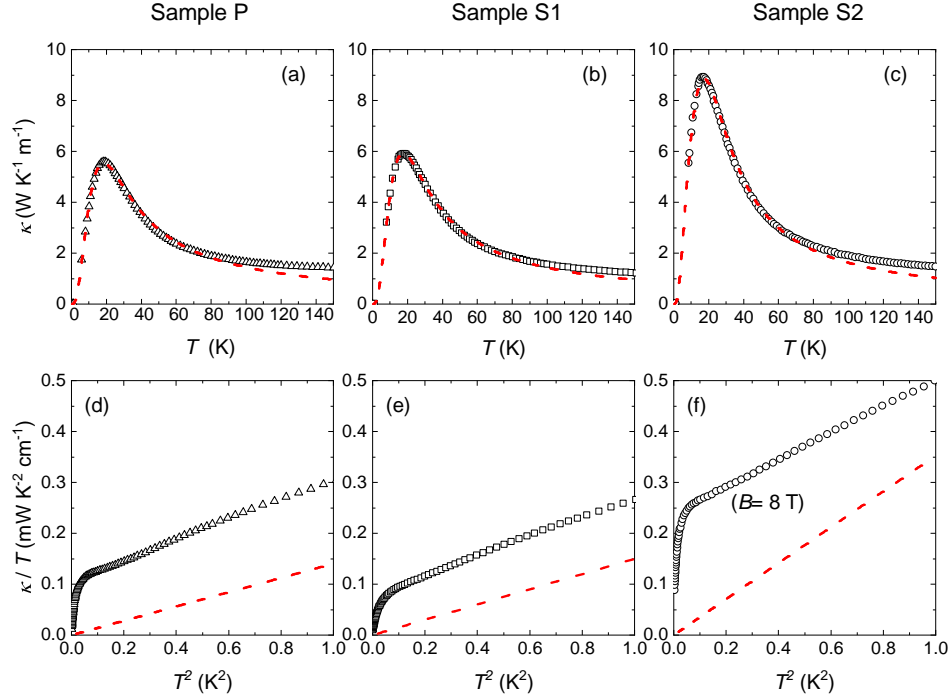


Fig. S4: Callaway fits to the higher-temperature thermal conductivity. Thermal conductivity κ in zero field above 6 K for the (a) polycrystalline Sample P, the single crystals (b) Sample S1, and (c) Sample S2. The red dashed lines represent the fitting results according to the Callaway model with a fitting range up to 100 K. Comparison between the estimated phononic thermal conductivity κ_{ph} according to the obtained parameters in Table S1 (red dashed line) and the measured low-temperature κ data of (d) Sample P at 0 T, (e) Sample S1 at 0T, and (f) Sample S2 at 8T (due to the additional low-temperature peak without field in this sample) are presented.

By extending the phonon model with the obtained fitting parameters to low temperatures ($T < 1$ K), one can directly compare the measured data with the phenomenologically expected phonon contribution. Fig. S4(d-f) show that the predicted low-temperature phonon heat conductivity is significantly smaller than the measured κ , where is very similar to the measured data at $T^2 > 0.1$ K². In view of the fact that there is some error margin due to different geometry factors in different measurement setups, this agreement is very good. This not only corroborates our estimation of the phononic heat conductivity κ_{ph} from analyzing the T^3 term in the low- T data (see also below). It also confirms that the peculiar temper-

ature and field dependence is not produced by a phononic scattering behavior off magnetic excitations but rather by an additional direct contribution to the heat conductivity by a magnetic transport channel.

Note that the origin of the T^3 dependence is rooted in the direct proportionality of κ_{ph}/T with the phononic specific heat in the low- T limit. A precondition to observe it experimentally is that the phonons scatter diffusively off the crystal surfaces. A deviation from a T^3 behavior is usually attributed to the surface roughness of the sample that drives the sample towards the specular surface scattering limit [9]. In this context, we want to point out that some recent studies of low-temperature thermal conductivity properties of candidate quantum spin liquid materials reported field-dependent power-law behavior [10–12]. These observations of non- T^3 power-law $\kappa(T)$ can not be attributed only to the surface roughness since it should be field-independent. On the other hand, the fact that a moderate magnetic field can change the power-law exponent in these cases suggests the scattering of phonons is also contributed by the spin-phonon scattering. Please be aware that in our data there is no evidence for such effects which yield a deviation from T^3 in the heat conductivity of $\text{PbCuTe}_2\text{O}_6$.

V. Estimation of the spinon mean free path

The dynamical properties of spinon excitations are important for understanding the QSL states. Here we provide an estimation of the mean free path l_{spinon} of spinons in PbCuTeO_6 . The thermal conductivity of a mobile (quasi)particle is determined by

$$\kappa = 1/3 \times C \times v \times l, \quad (6)$$

where C , v and l are specific heat, the velocity and the mean free path of this (quasi)particle, respectively.

In the case of PbCuTeO_6 , a linear contribution is not observed in the heat capacity measurement in the sub-Kelvin regime [2, 3]. In contrast, the dominating feature is a pronounced anomaly at about 1 K which signals the ferroelectric transition. A possible explanation is that the entropy associated with this transition obscures the magnetic specific heat but does not contribute to the heat transport because of a non-dispersive character of the dipole fluctuations. Note also that the related structural distortion is very subtle with

relative axes length changes of the order of $\sim 10^{-6}$, see Ref [13]. This provides a further explanation for the absence of any signatures of the transition in the thermal conductivity, even for measurements extending above 1 K.

In order to estimate l_{spinon} we therefore rely on recent theoretical results for C_{spinon} for a possible gapless QSL state in hyper-hyper-kagome systems [14], where $C_{\text{spinon}}/T \approx 2.5k_B^2/J$ per spin is estimated. By taking the $J = 1.13$ meV and structural parameters for PbCuTeO_6 [1], $C_{\text{spinon}}/T = 1.6$ mJ/(K²mol). To evaluate v_{spinon} , one can also refer to the Fermi surface properties calculated within the same theoretical work [14]. By taking their results of the ground state with a spinon Fermi surface, $\epsilon_F = 0.0574J$, $k_F \sim 0.35 \times 2\pi/d$, and $e(k) = \hbar v_{\text{spinon}}k$ [14], v_{spinon} is estimated to be 123 m/s. In this way, the l_{spinon} of PbCuTeO_6 is estimated to be 133 Å (Sample S1), 434 Å (Sample S2), and 177 Å (Sample P), corresponding to 30, 99, and 41 spin spacings (d_{S-S}), respectively. We summarize these values in Table S2 together with results for other QSL candidate materials found in the literature.

Material [Reference]	l_{spinon} [Å]	$l_{\text{spinon}}/d_{S-S}$
$\text{PbCuTe}_2\text{O}_6$ (Sample S1) [this work]	133	30
$\text{PbCuTe}_2\text{O}_6$ (Sample S2) [this work]	434	99
$\text{PbCuTe}_2\text{O}_6$ (Sample P) [this work]	177	41
$\text{EtMe}_3\text{Sb}[\text{Pd}(\text{dmit})_2]_2$ [15]	10^4	1000
$\text{Cu}_3\text{V}_2\text{O}_7(\text{OH})_2 \cdot 2\text{H}_2\text{O}$ (S1) [16]	230	80
$\text{Cu}_3\text{V}_2\text{O}_7(\text{OH})_2 \cdot 2\text{H}_2\text{O}$ (S2) [16]	690	240
$\text{Na}_2\text{BaCo}(\text{PO}_4)_2$ [17]	36.6	7
$1T-\text{TaS}_2$ [18]	$\gg 50$	$\gg 5$
YbMgGaO_4 [19]	78.4	23
$\text{BaCo}_2(\text{AsO}_4)_2$ [12]	123.8	43

Table S2: Estimation of the spinon mean free path l_{spinon} of some candidate spin liquid materials, and a comparison to their corresponding spin-spin distance d_{S-S} .

VI. A closer look at the thermal conductivity below T_{drop}

As mentioned in the main text, the depleted κ_{spinon} signal can either indicate a spinon excitation gap, or the loss of coupling between spinons and the phonon background [20], through which κ of an insulator is measured. We are aware that a \mathbb{Z}_2 QSL ground state with a gap value of $0.0259J$ was recently predicted for the $S = 1/2$ hyper-hyper-kagome QSL [14]. It matches remarkably well to our measured value for T_{drop} ($\approx 0.026J_1$). However, if T_{drop} indeed gauges a spinon excitation, its field dependence (see Fig. 3 of the main text) is unusual since the spin excitation gap in frustrated magnets naively should first close in field [21, 22].

If one assumes a spinon-phonon decoupling does not take any role in the temperature range covered by this study, the critical information about whether the spinon Fermi surface is fully gapped or has some "nodes" should be encoded in the details of the $\kappa_{\text{spinon}}(T)$ data below T_{drop} . Both power-law ($\kappa_{\text{spinon}} = b \times T^n$, corresponding to a nodal spinon Fermi surface) and exponential ($\kappa_{\text{spinon}} = A \times e^{-\Delta/k_B T}$, corresponds to fully-gapped spinon Fermi surface) fit to the representative extracted $\kappa_{\text{spinon}}(T)$ data, see Fig. S6. None of them can reproduce the data in the whole temperature range very well in their simplest form. The exponential fit yields a gap $\Delta/k_B \approx 140$ mK, i.e., a gap value which is about a factor of 2.5 smaller than the theoretically expected value [14].

On the other hand, if the κ_{spinon} depletion results from spinon-phonon decoupling, there exists a phenomenological model that successfully described the downturn of electronic κ_e/T in a cuprate [20]: $T_{\text{drop}} \propto a^{1/(n-1)}$, where a is the κ_{spinon} residual linear term and n is a fitting parameter between 4 and 5 [20]. Since a similar consideration for spinon-phonon coupling is still missing to our knowledge, and assuming the equivalence of electron and spinon in this setting, we compare below our observations for Sample S1 and Sample P (for Sample S2, the downturn is not observed) with the predictions of this model.

In Fig. S7 the relationship of T_{drop} and the residual linear term a is displayed in log-log scale. According to the decoupling model [20],

$$T_{\text{drop}} = (a/Kl_s^2)^{1/(n-1)} \quad (7)$$

where K is a constant which depends on the electron-phonon interaction matrix element, l_s is the length of the sample along the current direction, and n is a fitting parameter between 4 and 5 [20]. For a logarithmic presentation, Eq. 7 is converted into

$$\log a = (n - 1) \log T_{\text{drop}} + \log(Kl_s^2), \quad (8)$$

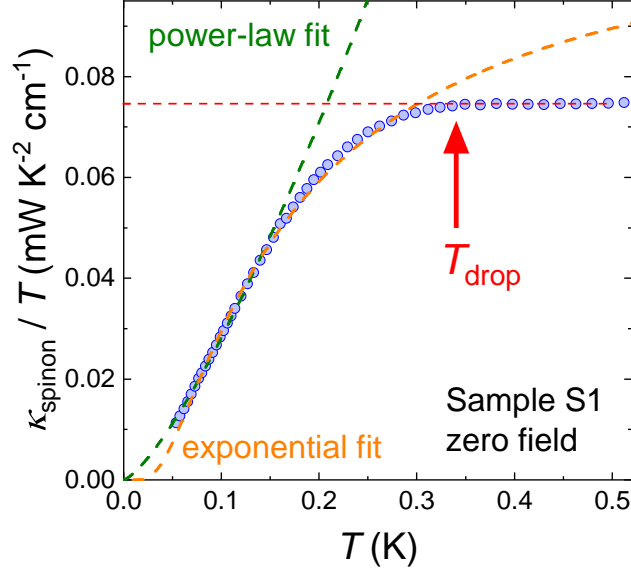


Fig. S6: Temperature dependence of spinon thermal conductivity in the form of κ_{spinon}/T , acquired by subtracting the phononic contribution from the total κ/T . Below a critical temperature $T_{drop} \approx 340$ mK, highlighted by the red arrow, κ_{spinon}/T starts to drop to zero. The green and orange dashed lines are power-law and exponential fits to the data in the lowest temperature range. Data corresponds to Sample S1 in zero field, see Fig. 1(a) of the main text.

where the $\log(Kl_s^2)$ term is a constant for a given sample. Especially, K should not fundamentally change for a given material and l_s is comparable for Sample P and Sample S1 (see Section I: Sample preparation). Hence, all the field dependent data of both samples are expected to be on the same line with a slope between $n = 4$ and $n = 5$. However, as can be seen in Fig. S7, the data do not follow such behavior, even for one given sample.

We have to mention that our analysis does not rule out the spinon-phonon decoupling as a feasible explanation for the decay of κ/T at the low temperature limit. But a considerable modification of the original model [20] needs to be implemented in order to make it compatible with the observations.

Future work is required to clarify which of these two scenarios is valid. In any case, either of these scenarios will strongly impact the research on frustrated quantum magnets. A decoupling of phonons and spinons, if confirmed, will teach caution in the interpretation of ultra-low-temperature heat transport data. On the other hand, an experimental proof

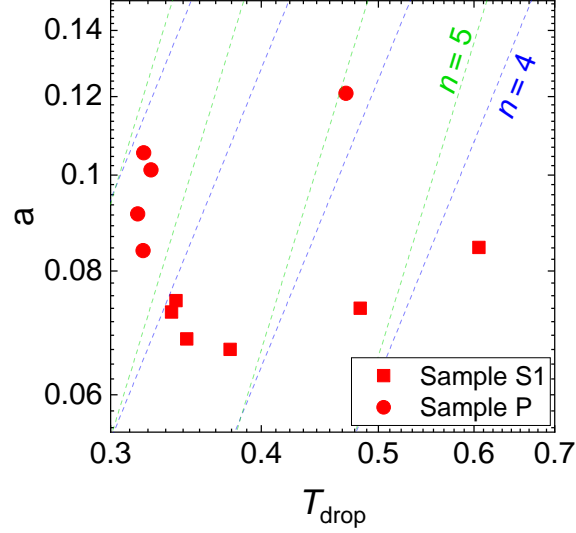


Fig. S7: The relationship between a and T_{drop} of Sample S1 (square) and Sample P (circle), in logarithmic plot. The data were obtained from the results at various magnetic fields. The dashed green and blue lines are indicating the slopes for $n = 5$ and $n = 4$ lines, respectively.

of a \mathbb{Z}_2 ground state would represent a new paradigm in quantum magnetism beyond the evidence of a spinon Fermi surface as revealed by our data for $T > T_{\text{drop}}$.

VII. Extended data shown as log-log plots and waterfall plots

In the main text, the temperature dependence of κ was mainly plotted in the form of κ/T against T^2 for clarify. A double-log plot of κ against T for viewing the power-law T dependence of κ in a more unbiased manner is provided by Fig. S8.

In Fig. S9 we plot a representative selection of these data. This representation reveals that the data are not compatible with a single power law. A T^3 behavior is only asymptotically reached at high temperature.

A different representation of the data of all samples as a function of temperature and magnetic field is shown in the waterfall plots in Fig. S10. Since our RuO_2 thermometers' sensitivity drops considerably with increasing temperature, the data above 1 K (and below 5 K) are regarded of lower accuracy, and thus we limited the data to $T \leq 1$ K in the main text. Still the data for $T > 1$ K yield valuable information. One can see more clearly that

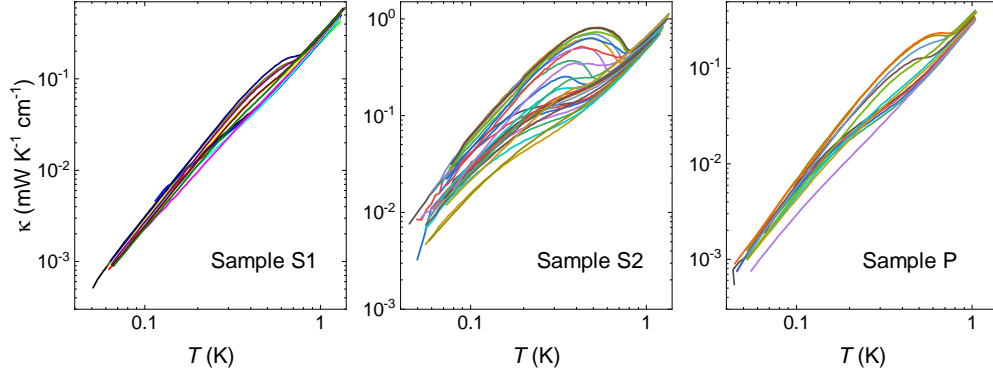


Fig. S8: Log-log plots of all low-temperature $\kappa(T)$ data for the three samples.

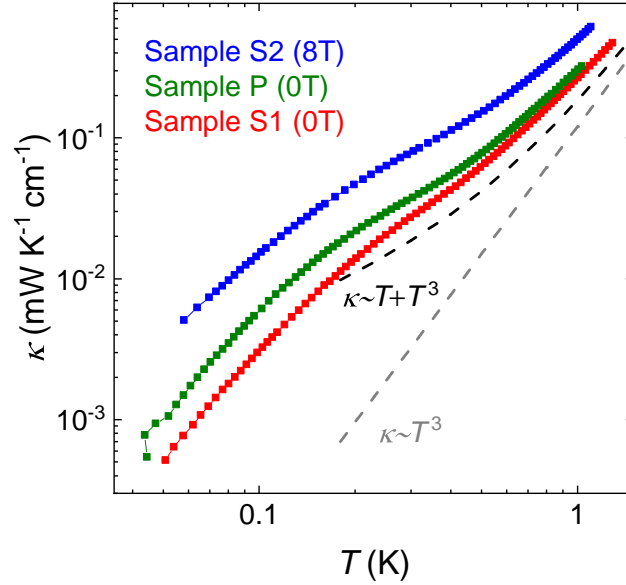


Fig. S9: Log-log plots of representative $\kappa(T)$ data of the three samples. Dashed lines stand for the typical T^3 behavior and a $T + T^3$ behavior.

the pronounced 1 K anomaly in specific heat has no observable effect in κ . Note that the related structural distortion of this 1 K ferroelectric transition is very subtle with relative axes length changes of the order of $\sim 10^{-6}$, see Ref [13]. This provides an explanation for the absence of any signatures of the transition in the thermal conductivity.

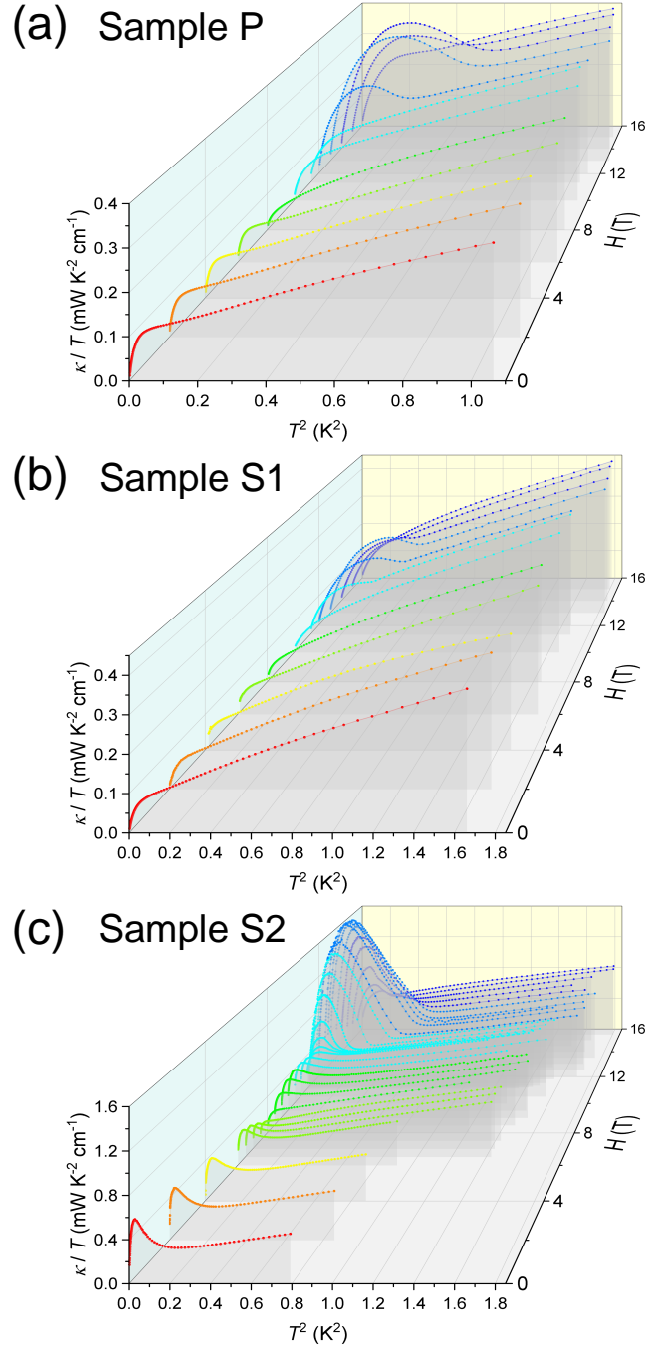


Fig. S10: Waterfall plots of the low-temperature thermal conductivity of (a) Sample P, (b) Sample S1, and (c) Sample S2.

VIII. More discussion on the additional lower-temperature $\kappa/T(T)$ peak

Despite the fact that magnetic order could not be detected below 11 T in previous works on $\text{PbCuTe}_2\text{O}_6$ samples [1–3, 8, 13, 23], we tend to attribute this feature to a magnetic order induced by inclusions. This is reasonable since muon spin relaxation and nuclear magnetic resonance data reveal a slowing down of spin fluctuations which imply the proximity of the system to magnetic order [23]. The critical nature is further confirmed by a diverging Grüneisen parameter [13]. Considering the non-magnetic $\text{Pb}_2\text{Te}_3\text{O}_8$ second phase inclusions of Sample S2 [2], one may therefore conjecture that weak sample-dependent magnetic order can be induced, if the fine balance between magnetic interactions is disturbed by strain fields around the inclusions of the second phase. Apparently, this specialty of Sample S2 together with the symmetry reduction connected with the structural phase transition and the ferroelectric order seems sufficient to tip the system towards magnetic order.

-
- [1] S. Chillal et al., *Evidence for a three-dimensional quantum spin liquid in PbCuTe₂O₆*, Nat. Commun. **11**, 2348 (2020).
- [2] A.R.N. Hanna et al., *Crystal growth, characterization, and phase transition of PbCuTe₂O₆*, Phys. Rev. Materials **5**, 113401 (2021).
- [3] P. Eibisch et al., *Field-induced effects in the spin liquid candidate PbCuTe₂O₆*, Phys. Rev. B **107**, 235133 (2023).
- [4] G. G. Ihas, L. Frederick, and J. P. McFarland, *Low Temperature Thermometry in High Magnetic Fields*, J. Low Temp. Phys. **113** 963–968 (1998).
- [5] R. Hentrich et al., *Unusual Phonon Heat Transport in α -RuCl₃: Strong Spin-Phonon Scattering and Field-Induced Spin Gap*, Phys. Rev. Lett. **120**, 117204 (2018).
- [6] J. Callaway, *Low-Temperature Lattice Thermal Conductivity*, Phys. Rev. **122**, 787 (1961).
- [7] J. Callaway, *Model for Lattice Thermal Conductivity at Low Temperatures*, Phys. Rev. **113**, 1046 (1959).
- [8] B. Koteswararao et al., *Magnetic properties and heat capacity of the three-dimensional frustrated $S = 1/2$ antiferromagnet PbCuTe₂O₆*, Phys. Rev. B **90**, 035141 (2014).
- [9] S. Y. Li et al., *Low-temperature phonon thermal conductivity of single-crystalline Nd₂CuO₄: Effects of sample size and surface roughness*, Phys. Rev. B **77**, 134501 (2008).
- [10] Q. Barthelemy et al., *Heat conduction in herbertsmithite: Field dependence at the onset of the quantum spin liquid regime*, Phys. Rev. B **107**, 054434 (2023).
- [11] X. C. Hong et al., *Phonon thermal transport shaped by strong spin-phonon scattering in a Kitaev material Na₂Co₂TeO₆*, on-line preprint at arXiv:2306.16963
- [12] C. P. Tu et al., *Evidence for gapless quantum spin liquid in a honeycomb lattice*, on-line preprint at arXiv:2212.07322
- [13] C. Thurn et al., *Spin liquid and ferroelectricity close to a quantum critical point in PbCuTe₂O₆*, npj Quantum Mater. **6**, 95 (2021).
- [14] L. E. Chern and Y. B. Kim, *Theoretical study of quantum spin liquids in $S = 1/2$ hyperkagome magnets: Classification, heat capacity, and dynamical spin structure factor*, Phys. Rev. B **104**, 094413 (2021).
- [15] M. Yamashita et al., *Highly mobile gapless excitations in a two-dimensional candidate quantum*

- spin liquid*, Science **328**, 1246 (2010).
- [16] D. Watanabe et al., *Emergence of nontrivial magnetic excitations in a spin-liquid state of kagome volborthite*, Proc. Natl. Acad. Sci. U.S.A. **113**, 8653-8657 (2016).
- [17] N. Li et al., *Possible itinerant excitations and quantum spin state transitions in the effective spin-1/2 triangular-lattice antiferromagnet Na₂BaCo(PO₄)₂*, Nat. Commun. **11**, 4216 (2020).
- [18] H. Murayama et al., *Effect of quenched disorder on the quantum spin liquid state of the triangular-lattice antiferromagnet 1T-TaS₂*, Phys. Rev. Research **2**, 013099 (2020).
- [19] X. Rao et al., *Survival of itinerant excitations and quantum spin state transitions in YbMgGaO₄ with chemical disorder*, Nat. Commun. **12**, 4949 (2021).
- [20] M. F. Smith et al., *Origin of anomalous low-temperature downturns in the thermal conductivity of cuprates*, Phys. Rev. B **71**, 014506 (2005).
- [21] X. C. Hong et al., *Heat transport of the kagome Heisenberg quantum spin liquid candidate YCu₃(OH)_{6.5}Br_{2.5}: Localized magnetic excitations and a putative spin gap*, Phys. Rev. B **106**, L220406 (2022).
- [22] M. Fu et al., *Evidence for a Gapped Spin-Liquid Ground State in a Kagome Heisenberg Antiferromagnet*, Science **350**, 655-658 (2015).
- [23] P. Khuntia et al., *Spin liquid state in the 3D frustrated antiferromagnet PbCuTe₂O₆: NMR and Muon spin relaxation studies*, Phys. Rev. Lett. **116**, 107203 (2016).